



Audio Engineering Society Convention Paper

Presented at the 136th Convention
2014 April 26–29 Berlin, Germany

This paper was peer-reviewed as a complete manuscript for presentation at this Convention. Additional papers may be obtained by sending request and remittance to Audio Engineering Society, 60 East 42nd Street, New York, New York 10165-2520, USA; also see www.aes.org. All rights reserved. Reproduction of this paper, or any portion thereof, is not permitted without direct permission from the Journal of the Audio Engineering Society.

On Spatial-Aliasing-Free Sound Field Reproduction using Infinite Line Source Arrays

Frank Schultz, Till Rettberg and Sascha Spors

Institute of Communications Engineering, University of Rostock, Germany

Correspondence should be addressed to Frank Schultz (frank.schultz@uni-rostock.de)

ABSTRACT

Concert sound reinforcement systems aim at the reproduction of homogeneous sound fields over extended audiences for the whole audio bandwidth. For the last two decades this has been mostly approached by using so called line source arrays due to their superior abilities of producing homogeneous sound fields. Design and setup criteria for line source arrays were derived as Wavefront Sculpture Technology in literature. This paper introduces a viewpoint on the problem at hand by utilizing a signal processing model for sound field synthesis. It will be shown that the optimal radiation of a line source array can be considered as a special case of spatial-aliasing-free synthesis of a wave front that propagates perpendicular to the array. For high frequencies the so called waveguide operates as a spatial lowpass filter and therefore attenuates energy that otherwise would lead to spatial aliasing artifacts.

1. INTRODUCTION

Wavefront Sculpture Technology¹ (WST) and its derived criteria [1, 2, 3] represent the modern fundamentals of *line source array* (LSA) radiation. Similar findings were also discussed in [4]. The WST criteria define how to engineer LSA elements (single loudspeaker cabinets) and how to setup an LSA in order to reproduce homogeneous sound fields over a large audience area. The WST criteria 1-3 [3, pg.

929] define how the LSA elements have to be designed to arrange an in-phase driven, straight LSA of finite length. For high frequencies (>1-2 kHz) the criteria require line pistons with specific length and infinitesimal width as individual sources. This will be achieved by a waveguide that is able to "generate a flat, isophasic" wavefront [3, pg. 916]. This feature constitutes the main difference to a *line array* for which regular (horn-loaded) loudspeakers are vertically stacked. Typically the latter produce undesired interference patterns – which we will term spatial aliasing – that corrupt the desired sound field mainly at high frequencies. LSA design aims to avoid this.

¹Wavefront Sculpture Technology[®] is a registered trademark of L-ACOUSTICS US, LLC. We omit the labeling in the remainder of the paper and will only use the relevant research results.

The WST criterion 4 defines an optimal array curvature to provide a homogeneous and frequency independent amplitude decay over the audience distance. The WST criterion 5 interrelates the length of the waveguide and a maximum possible splaying angle between the LSA elements. Model- or data based loudspeaker directivities have been taken into account for the prediction of sound fields generated by LSAs [5, 6, 7, 8, 9]. Radiation synthesis has been approached by solving an inverse problem using numerical optimization and driving the LSA elements with finite impulse response filters (FIR) [10, 11].

In this paper we approach the radiation synthesis problem analytically, by applying findings from the broader theory of sound field synthesis (SFS). Linear loudspeaker arrays have been discussed for Wave Field Synthesis (WFS) [12] and for the Spectral Division Method (SDM) [13]. Usually, the individual sources – termed *secondary sources* in SFS – are modeled as spherical monopoles, resulting in a simplified mathematical formulation. Approaches exist which also implement model- or data based loudspeaker directivities into SFS algorithms [14, 15, 16, 17, 18, 19].

We briefly revisit SFS theory and derive a suitable driving function for an LSA beginning with a continuous secondary source distribution (SSD). For clarity of analysis, spatial discretization [1, II.3.] and spatial truncation [20] of the LSA are treated separately. This paper’s scope is restricted to the spatial sampling process and its implications.

We propose an optimal waveguide design from a theoretical viewpoint which is in agreement with the known WST criteria 1,2. We will show that an ideal waveguide has a directivity which theoretically is able to suppress all spatial-aliasing components. The simulations are compared to measurements of a real waveguide. Spatial truncation and its interaction with discretization will be discussed in an upcoming study [21].

2. NOMENCLATURE

This section defines conventions and notations that are used throughout this study. The unit vector $\mathbf{e}_r = (\sin \varphi \sin \theta, \cos \varphi, \sin \varphi \cos \theta)$ with $\varphi \in [0, \pi]$ and $\theta \in [0, 2\pi)$ links the position vector $\mathbf{x} = (x, y, z) = \|\mathbf{x}\| \mathbf{e}_r$ with $\|\mathbf{x}\| = r = \sqrt{x^2 + y^2 + z^2}$ and the wave number vector $\mathbf{k} = (k_x, k_y, k_z) = \frac{\omega}{c} \mathbf{e}_r$

with $\frac{\omega}{c} = \sqrt{\langle \mathbf{k}, \mathbf{k} \rangle}$ by denoting the scalar product $\langle \cdot, \cdot \rangle$ and the speed of sound c in m/s. Note that the used spherical coordinate system has untypical nomenclature but is consistent with the representation of loudspeaker directivities known from textbooks, cf. (32),(33). A constant speed of sound $c=343$ m/s is assumed throughout this study. The dispersion relation $(\frac{\omega}{c})^2 = k_x^2 + k_y^2 + k_z^2$ holds. The scalar product notation $\langle \mathbf{k}, \mathbf{x} \rangle = k_x x + k_y y + k_z z$ is used for the description of plane waves in cartesian coordinates. The temporal angular frequency $\omega = 2\pi f$ in rad/s is linked to the temporal frequency f in Hz. The temporal Fourier transform sign and normalization convention $p(\mathbf{x}, t) = 1/(2\pi) \int P(\mathbf{x}, \omega) e^{+j\omega t} d\omega$ is used for the relationship of the sound pressure $p(\mathbf{x}, t)$ in time domain and its temporal spectrum $P(\mathbf{x}, \omega)$ by denoting the unit imaginary number j . The spatial Fourier transform sign and normalization convention $P(x, \omega) = 1/(2\pi) \int P(k_x, \omega) e^{-jk_x x} dk_x$ is used. This implies that the wave vector \mathbf{k} denotes the propagation direction of the wave. Thus $e^{-j \langle \mathbf{k}_{PW}, \mathbf{x} \rangle} e^{+j\omega_{PW} t}$ describes a unit amplitude monochromatic plane wave which propagates into direction of \mathbf{k}_{PW} . For the chosen conventions the three-dimensional, freefield Green’s function is defined by $G(\mathbf{x}, \mathbf{x}_0, \omega) = \frac{e^{-j \frac{\omega}{c} \|\mathbf{x} - \mathbf{x}_0\|}}{4\pi \|\mathbf{x} - \mathbf{x}_0\|}$ with the source position \mathbf{x}_0 [22, 27.4]. It models a spherical monopole [23, ch. 5.16]. For brevity, dependence on the temporal angular frequency ω is omitted.

3. SOUND FIELD REPRODUCTION

A well known approach for sound field prediction of a finite LSA [9] is based on the complex summation over N LSA elements which are defined by their individual farfield directivity patterns $A_n(\varphi, \theta, \omega)$ and a complex temporal frequency dependent weighting $D(\mathbf{x}_0, n, \omega)$. This filter defines magnitude, phase and delay for the individual secondary sources and is termed *driving function* in SFS.

For discrete source positions \mathbf{x}_0, n we can therefore write, cf. [9, (11)], [24, (2)]

$$P(\mathbf{x}) = \sum_{n=1}^N D(\mathbf{x}_0, n) A_n(\mathbf{x}, \mathbf{x}_0, n) \frac{e^{-j \frac{\omega}{c} \|\mathbf{x} - \mathbf{x}_0, n\|}}{4\pi \|\mathbf{x} - \mathbf{x}_0, n\|}. \quad (1)$$

While this equation is useful for the prediction of sound fields and constitutes the basis for numerical

optimization schemes, it does not reveal how spatial aliasing is generated. Since we are majorly interested in this question the problem is reformulated and simplified in the first instance. We are then able to show under which circumstances spatial aliasing in LSA setups occurs and how to avoid it. This is achieved by spatially sampling the continuous problem formulation and a transformation into the wave number domain.

3.1. 2.5D Sound Field Synthesis

We start our discussion with the fundamentals of SFS. The sound field $P(\mathbf{x})$ produced from an infinite, continuous, linear array is described by the single layer potential (SLP)

$$P(\mathbf{x}) = \int_{-\infty}^{+\infty} D(\mathbf{x}_0) G(\mathbf{x}, \mathbf{x}_0) dx_0 \quad (2)$$

using the driving function $D(\mathbf{x}_0)$ and the Green's function $G(\mathbf{x}, \mathbf{x}_0)$. The following conventions are chosen: the SSD, i.e. the infinite, linear, continuous array is located on the x -axis $\mathbf{x}_0 = (x_0, 0, 0)$. Such a linear source is incapable of radiating three dimensional plane waves and rather emits cylindrical waves [13, III.B]. This mismatch between a linear SSD (2D problem) and the employed Green's function (3D solution of the inhomogeneous wave equation) is treated in so called 2.5D SFS [12]. Thus our

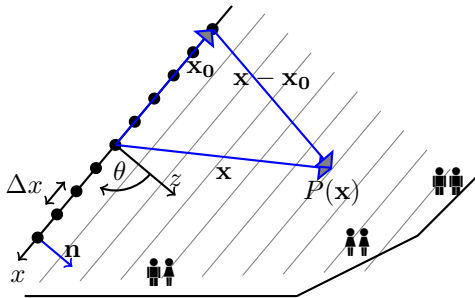


Fig. 1: Side view of the simplified SSD setup for a typical multi-stand public address situation. The infinite SSD is located on the x -axis. Sound field reproduction is considered within the xz -plane ($z > 0$). The SSD becomes continuous for a secondary source spacing $\Delta x \rightarrow 0$. The LSA is later modeled by spatially sampling the driving function and exchanging the Green's function in (2).

target space for sound reinforcement is the half plane $\mathbf{x} = (x, 0, z)$ with $z > 0$ for which $\varphi = \pi/2$ holds. In fig. 1 the utilized geometry and the simplified setup are depicted.

For uniform SSD characteristics, the Green's function is shift-invariant and (2) can be interpreted as a convolution along x with $z = \text{const}$

$$P(\mathbf{x}) = D(\mathbf{x}|_{y=0}) *_x G_0(\mathbf{x}), \quad (3)$$

using the Green's function $G_0(\mathbf{x})$ in the coordinate system origin $\mathbf{x}_0 = \mathbf{0}$. This corresponds to a multiplication in the so called angular spectrum domain with respect to the wave number k_x , cf. [13],[25]

$$P(k_x, 0, z) = D(k_x, 0, z) \cdot G_0(k_x, 0, z), \quad (4)$$

using the one-dimensional spatial Fourier transform

$$P(k_x, y, z) = \int_{-\infty}^{+\infty} P(x, y, z) e^{+j k_x x} dx \quad (5)$$

along x . The unknown driving function is derived by division of the known functions, i.e. the desired sound field to be reproduced and the Green's function, within the angular spectrum domain. In order to do that $G_0(k_x, 0, z) \neq 0$ is required. A subsequent inverse Fourier transformation yields the driving function

$$D(x_0) = \frac{1}{2\pi} \int_{-\infty}^{+\infty} \underbrace{\frac{P(k_x, 0, z)}{G_0(k_x, 0, z)}}_{D(k_x, 0, z)} e^{-j k_x x} dk_x. \quad (6)$$

This approach is termed Spectral Division Method (SDM) in SFS literature, cf. [13, pg. 2040],[18].

We proceed with the derivation of a driving function $D(x_0)$ and its angular spectrum $D(k_x)$ for a wave radiation perpendicular to the line source. In our chosen geometry this requires the radiation only into $+z$ direction, for which $k_x = 0$, $k_y = 0$ and $k_z = \frac{\omega}{c}$ has to be chosen.

3.2. Derivation of the Driving Function

A thorough derivation of the driving function is found in [13, II. B] and is briefly revisited here. Let us assume the synthesis of a unit amplitude plane wave in the xz -half plane

$$P(x, 0, z, \omega) = e^{-j(\mathbf{k}_{\text{PW}}, \mathbf{x})} 2\pi \delta(\omega - \omega_{\text{PW}}) \quad (7)$$

with $\mathbf{k}_{\text{PW}} = (k_{x,\text{PW}}, 0, k_{z,\text{PW}})$ using $\varphi_{\text{PW}} = \pi/2$ and ω_{PW} as the desired temporal angular frequency. A spatial Fourier transform with respect to k_x yields

$$P(k_x, 0, z, \omega) = 2\pi \delta(k_x - k_{x,\text{PW}}) \times e^{-j k_{z,\text{PW}} \cdot z} \cdot 2\pi \delta(\omega - \omega_{\text{PW}}). \quad (8)$$

The spatial Fourier transform of the Green's function for propagating wave radiation is given as

$$G_0(k_x, 0, z, \omega) = -\frac{j}{4} H_0^{(2)} \left(\sqrt{\left(\frac{\omega}{c}\right)^2 - k_x^2} \cdot z \right), \quad (9)$$

where $H_0^{(2)}$ denotes the 0th order cylindrical Hankel function of 2nd kind [26, §10.1]. Note that we omit the discussion of evanescent waves. With the dispersion relation $k_z = \sqrt{\left(\frac{\omega}{c}\right)^2 - k_x^2}$ we can rewrite

$$G_0(k_x, 0, z, \omega) = -\frac{j}{4} H_0^{(2)}(k_z z). \quad (10)$$

The angular spectrum of the driving function follows from (6)

$$D(k_x, 0, z, \omega) = \frac{2\pi \delta(k_x - k_{x,\text{PW}}) \cdot e^{-j k_{z,\text{PW}} \cdot z}}{-\frac{j}{4} H_0^{(2)} \left(\sqrt{\left(\frac{\omega_{\text{PW}}}{c}\right)^2 - k_{x,\text{PW}}^2} \cdot z \right)} \times 2\pi \delta(\omega - \omega_{\text{PW}}). \quad (11)$$

It can be shown that the driving function does not reproduce a desired plane wave using a linear SSD. The sound field rather exhibits an amplitude decay proportional to $1/\sqrt{z}$ in the farfield which we identify as a cylindrical wave [13, (20)].

We proceed to derive the driving function's angular spectrum for our problem at hand. The desired propagation angles $\varphi_{\text{PW}} = \pi/2$ and $\theta_{\text{PW}} = 0$ define the wave vector $\mathbf{k}_{\text{PW}} = (0, 0, \frac{\omega_{\text{PW}}}{c})$. Then $k_{x,\text{PW}} = \sin \theta_{\text{PW}} \frac{\omega_{\text{PW}}}{c}$ and $k_{z,\text{PW}} = \cos \theta_{\text{PW}} \frac{\omega_{\text{PW}}}{c}$ hold and (11) simplifies to

$$D(k_x, 0, z, \omega) = \frac{2\pi \delta(k_x) \cdot e^{-j \frac{\omega_{\text{PW}}}{c} \cdot z}}{-\frac{j}{4} H_0^{(2)} \left(\frac{\omega_{\text{PW}}}{c} z \right)} \cdot 2\pi \delta(\omega - \omega_{\text{PW}}). \quad (12)$$

We may setup $z = z_{\text{REF}}$ in order to reproduce the exact amplitude of the actually desired plane wave at this line parallel to the SSD. For $\frac{\omega_{\text{PW}}}{c} z \gg 1$ the large

argument approximation of the Hankel function [26, 10.2.6] leads to the proportionality

$$\left| \frac{1}{-\frac{j}{4} H_0^{(2)} \left(\frac{\omega_{\text{PW}}}{c} z \right)} \right| \propto \left| \sqrt{\frac{\omega_{\text{PW}}}{c}} z \right|. \quad (13)$$

Hence, the driving function (12) inherently includes a 3 dB/oct. highpass filter for the case of our interest. For further discussion we omit the compensation filter and the phase shift $e^{-j \frac{\omega_{\text{PW}}}{c} \cdot z}$ in (12) and restrict the driving function's angular spectrum to

$$D(k_x, 0, z, \omega) = 2\pi \delta(k_x) \cdot 2\pi \delta(\omega - \omega_{\text{PW}}), \quad (14)$$

which yields the driving function

$$D(x_0, 0, z, \omega) = 1 \cdot 2\pi \delta(\omega - \omega_{\text{PW}}). \quad (15)$$

Eq. (15) confirms that an infinite, continuous line source driven with constant volume acceleration produces a cylindrical wave with a 3 dB/oct. lowpass behavior and a 3 dB level drop per distance doubling in the farfield, cf. [20, pg. 12]. In essence the 3 dB/oct. highpass (13) compensates the lowpass characteristics of the line source. In practical LSA applications this is referred to as the coupling filter, which is examined in detail in [21].

The angular spectrum of the desired full band driving function

$$D(k_x) = 2\pi \delta(k_x) \quad (16)$$

is depicted in fig. 2a, together with the farfield Green's function $G_0(k_x)$ (10). For a full audio-bandwidth wavefront into z -direction, $D(k_x)$ takes the shape of a vertical line. The propagating part of $G_0(k_x)$ is bounded to the triangular region where $|k_x| \leq \left|\frac{\omega}{c}\right|$. Then, each point coincident with $D(k_x)$ corresponds to a monochromatic cylindrical wave, as exemplarily shown for a single frequency in fig. 2b. Finally, the temporal-frequency lowpass behavior of a line source can be observed in the Green's function's magnitude along the line of $D(k_x)$ in fig. 2a.

3.3. Spatial Truncation of the Line Source

Practical arrays are obviously restricted to a finite length. This is realized by truncating the driving function with a spatial window $w(\mathbf{x}_0) \in \mathbb{R}$ in our signal processing model, cf. fig. 3. A thorough treatment of possible windowing artifacts in this context (i.e. leakage, near-/farfield characteristics [1]) is beyond the scope of this contribution. Truncation is

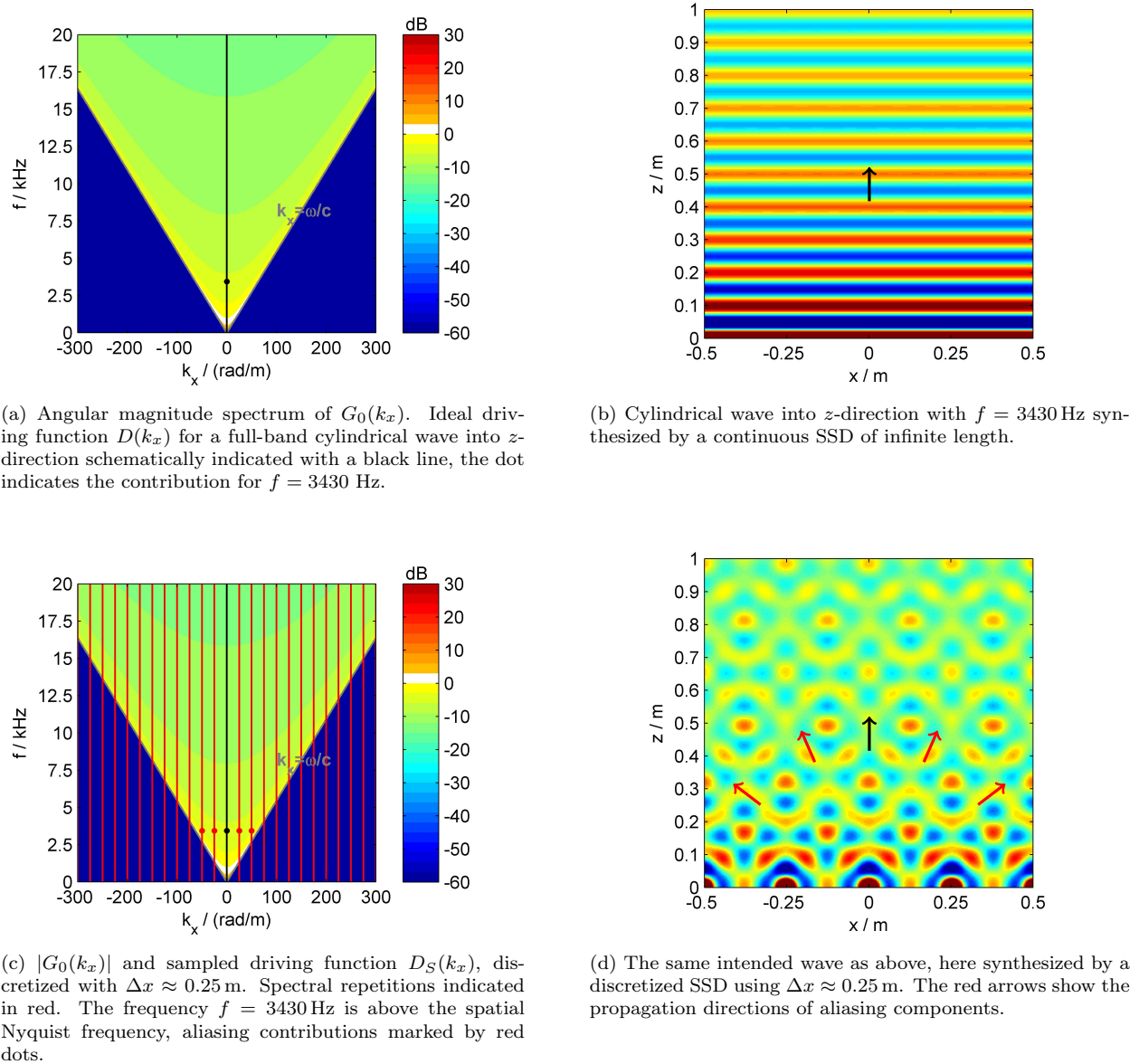


Fig. 2: Ideal sound field reproduction by a continuous SSD (top) and with spatial aliasing due to a discretized SSD (bottom). The angular spectra of the driving functions $D(k_x)$, $D_S(k_x)$ and of the Green's function $G_0(k_x)$ shown on the left. Magnitude of $G_0(k_x)$ in dB is normalized to $k_x = 0$ rad/m and $f = 1$ kHz with a 3 dB step colormap. Corresponding wave fields $\Re\{P(\mathbf{x})\}$ in the xz -plane for the frequency $f = 3430$ Hz are depicted on the right side.

to be discussed in detail in [21]. For concise argumentation, we consider only the discretization of

the SSD in the remainder of this paper and assume $w(x_0) = 1$.

3.4. Spatial Discretization of the Line Source

A continuous SSD cannot be realized in practice and is usually implemented as a linear array of discrete loudspeakers. This constitutes a spatial sampling process of the driving function as depicted in fig. 3. Assuming identical speakers, equidistantly arranged with Δx , ideal sampling is modeled by multiplication with an accordingly spaced Dirac comb. The discretized driving function $D_S(x_0)$ reads

$$D_S(x_0) = D(x_0) \cdot \underbrace{\sum_{\mu=-\infty}^{+\infty} \delta(x_0 - \mu \Delta x)}_{=: \frac{1}{\Delta x} \text{III}\left(\frac{x_0}{\Delta x}\right)}, \quad (17)$$

where the shorthand notation is obtained by dilating a Dirac comb $\text{III}(x_0) := \sum_{\mu=-\infty}^{+\infty} \delta(x_0 - \mu)$ [27, (11.1)] with unit spacing. The spatial Fourier transform pair for the Dirac combs (17) is known as

$$\underbrace{\sum_{\mu=-\infty}^{+\infty} \delta(x_0 - \mu \Delta x)}_{=: \frac{1}{\Delta x} \text{III}\left(\frac{x_0}{\Delta x}\right)} \circ \bullet \underbrace{\frac{2\pi}{\Delta x} \sum_{\mu=-\infty}^{+\infty} \delta\left(k_x - \mu \frac{2\pi}{\Delta x}\right)}_{=: \text{III}\left(\frac{k_x \Delta x}{2\pi}\right)}. \quad (18)$$

With [27, (11.33)]

$$D(x_0) \cdot \frac{1}{\Delta x} \text{III}\left(\frac{x_0}{\Delta x}\right) \circ \bullet \frac{1}{2\pi} D(k_x) *_{k_x} \text{III}\left(\frac{k_x \Delta x}{2\pi}\right) \quad (19)$$

we obtain the angular spectrum of the ideally sampled driving function

$$D_S(k_x, 0, z) = \frac{1}{\Delta x} \sum_{\mu=-\infty}^{+\infty} D(k_x - \mu \frac{2\pi}{\Delta x}). \quad (20)$$

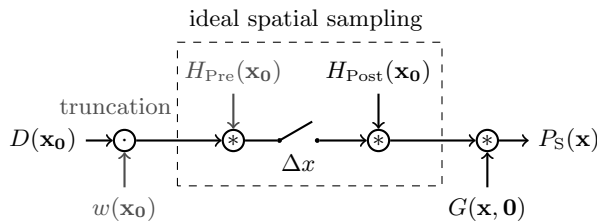


Fig. 3: The single layer potential for a linear, discretized and truncated SSD as a general signal processing model. Convolution is denoted by \circledast , multiplication by \circledcirc .

For our problem at hand we thus have to deal with the sampled version of (16)

$$D_S(k_x, 0, z) = \frac{2\pi}{\Delta x} \sum_{\mu=-\infty}^{+\infty} \delta(k_x - \mu \frac{2\pi}{\Delta x}). \quad (21)$$

In fig. 2c $D_S(k_x, 0, z)$ is schematically indicated for a spatially discretized SSD using a secondary source spacing of $\Delta x \approx 0.25$ m for which the spatial Dirac comb spacing $\Delta k_x = 2\pi/\Delta x = 25$ rad/m holds. Compared to fig. 2a the additional repetitions in the angular spectrum stemming from the Dirac comb are clearly indicated. Their coincidences with non-zero values of the Green's function indicate additional propagating contributions in the reproduced sound field. This is called spatial aliasing.

The radiating angles $\theta_{\mu \neq 0}$ of the spatial aliasing wave fronts are derived with $\sin \theta_{\mu \neq 0} = k_{x, \mu \neq 0} / \frac{\omega}{c}$ and are strongly dependent of the temporal angular frequency ω . Note that only for $|k_x / \frac{\omega}{c}| \leq 1$ propagating waves will be triggered. For frequencies smaller than

$$f < \frac{c}{\Delta x (1 + |\sin \theta|)} \quad (22)$$

no propagating spatial aliasing components will be synthesized, cf. [13, (38)]. For our problem at hand $\theta = 0$ eq. (22) reduces to

$$f < \frac{c}{\Delta x} \leftrightarrow \Delta x < \lambda \quad (23)$$

denoting the wavelength λ in m, cf. [1, sec. II.3.a]. Note that this criterion is different from that found in [3, sec. 3.1] for a discretized linear array of *finite* length ($\Delta x < \lambda/2$, WST #2). In [1, II.3.a.] an equivalent derivation is given and the resulting sound field was named "chaotic", although this term is somewhat misleading since the aliasing contributions can be analytically specified, at least for the considerations of an infinite array.

In contrast to the example in fig. 2b, for a spatially discretized SSD ($\Delta x \approx 0.25$ m) a propagating sound field for $f = 3430$ Hz is synthesized which consists of the desired cylindrical wave into k_z -direction plus four weighted spectral repetitions at $\mu = \pm 1, \pm 2$ in (21). The radiating angles of the additional cylindrical waves are derived to $\theta_{\mu=\pm 1, 2} = \pm 23.4^\circ, \pm 52.7^\circ$. The resulting sound field is depicted in fig. 2d. The

originally intended wave (cf. fig. 2b) is corrupted due to destructive and constructive interferences with the additional waves. The chosen SSD discretization does not allow the reproduction of a homogeneous wave at this frequency.

Spatial aliasing should obviously be avoided for uniform sound reinforcement in the listening area. We therefore need a methodology to suppress the spatial repetitions in the driving function's angular spectrum (21). This will be elaborated in the next sections.

3.5. Pre-/Postfilter for the Ideal Sampling Model

In classical baseband sampling theory the prefilter $H_{\text{Pre}}(x_0)$ and the postfilter $H_{\text{Post}}(x_0)$ in fig. 3 are usually understood as the anti-aliasing and the reconstruction filter, both with ideal spatial lowpass characteristics. When sampling the driving function, $H_{\text{Pre}}(x_0)$ ideally suppresses all contributions for $|k_x| > \pi/\Delta x$ (i.e. above the Nyquist frequency) to ensure a correctly sampled baseband. Subsequently, the ideal postfilter $H_{\text{Post}}(k_x)$ removes all spectral repetitions in $D_s(k_x)$ for correct baseband reconstruction. Artifacts due to a non-ideal prefilter have been termed *aliasing error* or *pre-aliasing*, those due to the postfiltering stage *reconstruction error* or *post-aliasing*, cf. [28]. In the context of SDM theoretical spatial postfiltering schemes were discussed in [18, 29].

In most practical SFS applications and radiation synthesis approaches however, explicit spatial pre- and postfiltering is omitted (i.e. $H_{\text{Pre}}(k_x) =$

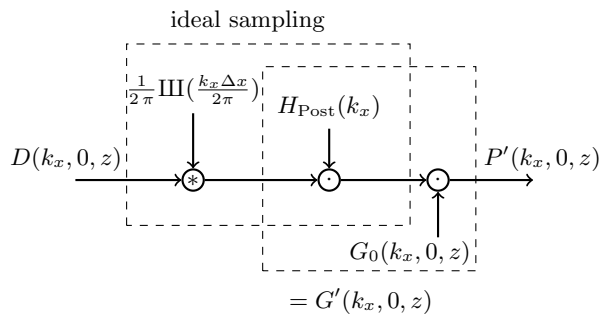


Fig. 4: The single layer potential for a linear, discretized SSD with the postfilter in the angular spectrum domain. The prefilter- and truncation stages are omitted.

$H_{\text{Post}}(k_x) = 1$). For our radiation problem at hand, dropping the prefilter is well justified: the continuous driving function $D(k_x)$ in (16) is already spatially band-limited and pre-aliasing cannot occur.

Omitting the postfilter on the other hand is not recommended: By (4), (10) and (21) the sound field $P(k_x)$ is reproduced as a product of the two functions $D_S(k_x)$ and $G_0(k_x)$ which both exhibit infinite spatial bandwidth. This results in post-aliasing as illustrated in fig. 2d. Therefore we aim for a spatial lowpass postfilter in the angular spectrum. The corresponding sampling model is shown in the block diagram in fig. 4.

With (4) and (21) we deduce

$$P'(k_x, 0, z) = \overbrace{D_S(k_x, 0, z)}^{\text{ideal sampling}} \cdot \underbrace{H_{\text{Post}}(k_x)}_{\text{loudspeaker as spatial lowpass}} \cdot G_0(k_x, 0, z) \quad (24)$$

(cf. [18, (36)]) and may define

$$G'(k_x, 0, z) = H_{\text{Post}}(k_x) \cdot G_0(k_x, 0, z) \quad (25)$$

which we term *Green's-like function*². The postfilter is split from the sampling stage and merged with the Green's function. This allows us to model an ideally sampled driving function and take loudspeaker farfield directivities into account, cf. (1). In practice the used loudspeakers exhibit a finite spatial bandwidth and thus operate as a (non-ideal) reconstruction filter. This method was also used in [14, 15, 18]. In [29, sec. 3.1] theoretical spatial lowpass secondary sources were discussed and denoted $G_{\text{anti-alias}}$.

We proceed with the derivation of Green's-like functions for baffled piston models which will serve for further examination of our problem.

4. PISTON GREEN'S-LIKE FUNCTIONS

The farfield radiation characteristics of a plane baffled piston is derived from the Rayleigh integral's

²Note that this is not a Green's function by strict definition, rather a particular solution of the wave equation with a different inhomogeneity $\neq \delta(\mathbf{x} - \mathbf{x}_0)$. We have chosen the term to stress its role of a propagator into space. Informally speaking, G' does for a loudspeaker modeled with farfield directivity what G_0 does for monopoles.

farfield approximation [22, (26.4)], [25, (2.84)]

$$P_{\text{Far}}(\mathbf{x}) = 2j\omega\rho_0 G(\mathbf{x}, \mathbf{x}_0) \times \int_{-\infty}^{+\infty} V_n(\mathbf{x}_0) e^{+j(k_x x_0 + k_y y_0)} dx_0 dy_0. \quad (26)$$

for which $\frac{\omega}{c} \|\mathbf{x} - \mathbf{x}_0\| \gg 1$. The piston is located in the xy -plane, thus $\mathbf{x}_0 = (x_0, y_0, 0)$. The field points are denoted by $\mathbf{x} = (x, y, z > 0)$. The nominal atmospheric density is denoted by ρ_0 in kg/m^3 . We use the piston's normal velocity temporal spectrum $V_n(\mathbf{x}_0)$ into z -direction. With (5) the integral in (26) is identified as the two-dimensional spatial Fourier transform $V(x, y, 0) \circ \bullet V(k_x, k_y, 0)$ and therefore

$$P_{\text{Far}}(\mathbf{x}) = 2j\omega\rho_0 G(\mathbf{x}, \mathbf{x}_0) V(k_x, k_y, 0). \quad (27)$$

We extend (27) with the complex source strength temporal spectrum, sometimes referred to as the volume flow Q [23, pg. 175], [22, ch. 18.3]

$$P_{\text{Far}}(\mathbf{x}) = 2Qj\omega\rho_0 G(\mathbf{x}, \mathbf{x}_0) \underbrace{\frac{V(k_x, k_y, 0)}{Q}}_{H(k_x, k_y)} \quad (28)$$

and define the dimensionless directivity function $H(k_x, k_y)$ [22, (26.7)]. The freefield Green's function is usually interpreted as a velocity potential stemming from a unit source, so (28) is rewritten accordingly:

$$\Phi_{\text{Far}}(\mathbf{x}) = 2Q G(\mathbf{x}, \mathbf{x}_0) H(k_x, k_y) \quad (29)$$

using $P(\mathbf{x}) = j\omega\rho_0 \Phi(\mathbf{x})$ [22, ch. 13.8]. For our half-space problem at hand, the volume flow is normalized to $Q = 1/2 (\text{m}^3/\text{s})/\text{Hz}$ to be consistent with the unit volume flow of the freefield (full space) Green's function. The Green's-like function for our 2.5D SFS problem – we only consider k_x – then reads

$$\Phi_{\text{Far,unitQ}}(\mathbf{x}) = G'(\mathbf{x}, \mathbf{x}_0) = G(\mathbf{x}, \mathbf{x}_0) \cdot H(k_x) \quad (30)$$

and the spatial Fourier transform with respect to x simply yields

$$G'(k_x, 0, z) = G_0(k_x, 0, z) \cdot H(k_x) \quad (31)$$

using (10). We recognize (31) as (25) with $H(k_x) = H_{\text{Post}}(k_x)$, that we previously interpreted as the

product of the freefield Green's function and a spatial postfilter. Also recall that $k_x = \frac{\omega}{c} \sin \theta$, so $H_{\text{Post}}(k_x)$ could be denoted as a function of θ as well, which is a more familiar representation of loudspeaker directivity patterns.

A single spherical monopole located at $\mathbf{x}_0 = \mathbf{0}$ features a postfilter $H_{\text{Monopole}}(k_x) = 1$.

A baffled circular piston with radius r_0 ($r_0^2 = x_0^2 + y_0^2$) located in the xy -plane and driven with constant velocity is described by the postfilter [22, (26.42)], [23, (7.4.17)]

$$H_{\text{Circ}}(k_x) = \frac{2J_1(k_x r_0)}{k_x r_0} = \frac{2J_1(\frac{\omega}{c} \sin \theta r_0)}{\frac{\omega}{c} \sin \theta r_0}, \quad (32)$$

where $J_1(\cdot)$ denotes the cylindrical Bessel function of 1st kind of 1st order [26, (10.2.2)].

A baffled linear piston of length L and infinitesimal width located at $|x_0| \leq L/2$ with constant velocity is characterized by the postfilter [22, (26.44)], [23, (7.3.3)]

$$H_{\text{Rect}}(k_x) = \frac{\sin(k_x \frac{L}{2})}{k_x \frac{L}{2}} = \frac{\sin(\frac{\omega}{c} \sin \theta \frac{L}{2})}{\frac{\omega}{c} \sin \theta \frac{L}{2}}. \quad (33)$$

5. IDEAL INFINITE LINE SOURCE ARRAY

We now discuss LSA design criteria for spatial-aliasing-free sound field reproduction. Recall our problem at hand using (21) and (24) for a desired spatial-aliasing-free cylindrical wave into z -direction, i.e. $k_x = 0$, $k_y = 0$, $k_z = \frac{\omega}{c}$.

Tab. 1 indicates the frequency range for discretized SSDs. We recognize that the spacing between secondary sources must not exceed a few mm to reproduce a full band spatial-aliasing-free sound field, cf. [3, pg. 918]. This is not a feasible approach. Instead of, an LSA element is designed with electrodynamic loudspeakers for the low and mid frequencies and employs a waveguide for the high frequencies.

5.1. Reproduction with Circular Pistons

We model an electrodynamic loudspeaker for $\lambda > r_0$ with a circular piston using the reconstruction filter (32). Circular pistons with radius $r_0 = 15''/2$ and $r_0 = 6.5''/2$ as indicated in tab. 1 are discussed due to their practical usage for LSA element designs.

In fig. 5a, 5b the Green's-like functions $G'_{\text{Circ}}(k_x)$ are

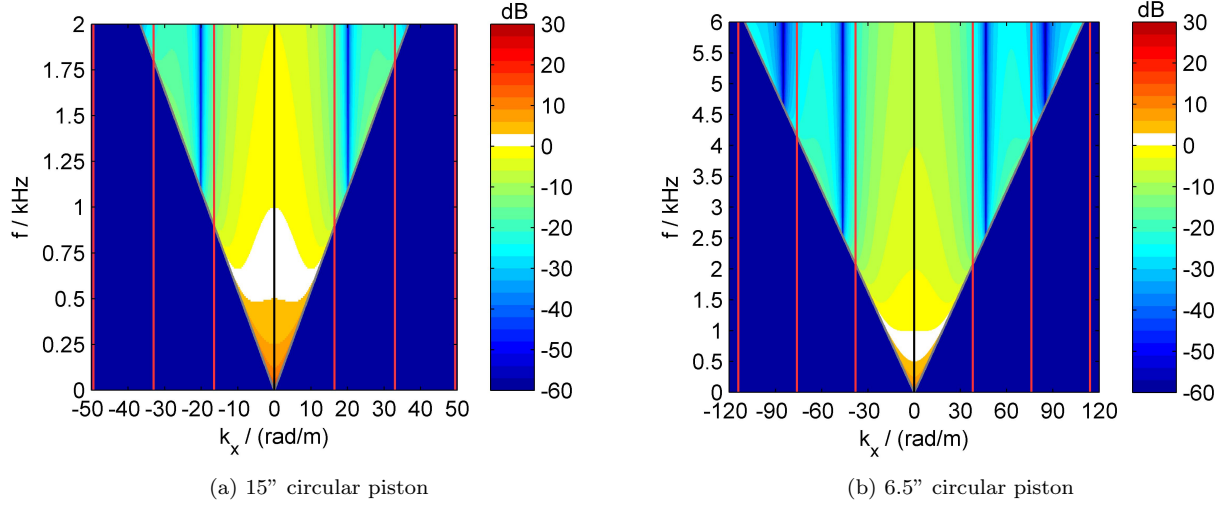


Fig. 5: $|G'_{\text{circ}}(k_x)|$ for two circular pistons with radius $r_0 = 0.1905$ m (left) and $r_0 = 0.08255$ m (right). $|G'_{\text{circ}}(k_x)|$ exhibits spatial lowpass characteristics. Sampled driving function' angular spectrum $D_S(k_x)$ with $\Delta x = 2r_0 \leftrightarrow \Delta k_x = \frac{2\pi}{\Delta x}$ indicated by vertical lines. Note the scaling of the frequency axis.

depicted in the angular spectrum domain. They feature the directivity pattern of (32) compared to the spherical monopole in fig. 2a. The amplitude decay w.r.t increasing $|k_x|$ indicates spatial lowpass characteristics. The Green's-like function will be triggered by the spectral repetitions of the sampled driving function's angular spectrum $D_S(k_x)$ (21). Due to the spatial lowpass, repetitions are attenuated. This produces a sound field with less spatial aliasing. In order to avoid it completely, band limitation in the temporal frequency domain has to be applied to the driving function, cf. [29, sec. 3.1.2]. In our ideal examples this would require a temporal frequency low-

pass with cut frequencies at 900 Hz and 2078 Hz respectively. For multi-way loudspeaker designs band-pass crossovers are employed. In real applications the crossover lowpass frequency is much lower than the critical anti-aliasing frequency (tab. 1) due to electro-acoustical concerns. We therefore conclude that the WST criterion 2 for perfect spatial-aliasing suppression is uncritical for the low and mid frequencies.

5.2. Reproduction with an Ideal Waveguide

Since the required small distances between the secondary sources for high frequencies are not feasible, waveguides were introduced in the literature [2, fig. 11]. Recall that we want to realize the driving function $D(x_0) = 1$ (15). From [1, I.3.] and [3, fig. 6] we deduce that a waveguide can be modeled as a line piston of length L . The resulting driving function using waveguides is piece-wise constant with amplitudes $D(x_0) \in \{0, 1\}$. This is illustrated in fig. 6 and represents the reconstructed driving function $D_{S,\text{Rect}}(x_0)$. A similar visualization was used in [3, fig. 6] to motivate waveguide modeling.

We proceed to derive $D_{S,\text{Rect}}(x_0)$ analytically. The postfilter $H_{\text{Post}}(x_0) = H_{\text{Rect}}(x_0)$ is expressed as the rect-function, cf. [27, (9.19)]

$\Delta x = 15'' = 0.381$ m	$f_{\text{no aliasing}} < 900$ Hz
$\Delta x = 6.5'' = 0.1651$ m	$f_{\text{no aliasing}} < 2078$ Hz
$\Delta x = 3'' = 0.0762$ m	$f_{\text{no aliasing}} < 4501$ Hz
$\Delta x = 1'' = 0.0254$ m	$f_{\text{no aliasing}} < 13504$ Hz

Table 1: Anti-aliasing condition (23) for a discretized SSD that should reproduce a cylindrical wave front perpendicular to the SSD. Δx indicates the theoretically minimum possible spacing between circular membranes of radius $\Delta x/2$.

$$H_{\text{Rect}}(x_0) = \text{rect}\left(\frac{x_0}{L}\right) = \begin{cases} 1 & \text{for } |x_0| \leq \frac{L}{2} \\ 0 & \text{else} \end{cases} \quad (34)$$

and is convolved with the ideally sampled driving function $D_S(x_0)$ (17), cf. fig. 3. This can be written

$$D_{\text{S,Rect}}(x_0) = \left[1 \cdot \sum_{\mu=-\infty}^{+\infty} \delta(x_0 - \mu \Delta x) \right] *_x \text{rect}\left(\frac{x_0}{L}\right). \quad (35)$$

The Dirac comb stemming from $D_S(x_0)$ (fig. 6, red) is 'smoothed' by the convolution with the rect-function yielding $D_{\text{S,Rect}}(x_0)$ (fig. 6, blue). By splitting the postfilter from the sampling process and merging it with the Green's function (cf. (25)) we see that the Green's-like function becomes an ideal, baffled, linear piston with length L and constant potential, instead of an ideal monopole.

From fig. 6 we graphically deduce that the driving function $D(x_0) = D_{\text{S,Rect}}(x_0) = 1$ is perfectly reconstructed for $L = \Delta x$ as intended for spatial-aliasing-free sound field reproduction. This is proven within the angular spectrum domain: With the spatial Fourier transform

$$H_{\text{Rect}}(k_x) = L \underbrace{\frac{\sin\left(\frac{k_x L}{2}\right)}{\frac{k_x L}{2}}}_{=: \text{sinc}\left(\frac{k_x L}{2}\right)} \quad (36)$$

[27, (9.24)] we re-identify the stated Green's-like function (33). Note the normalization mismatch by

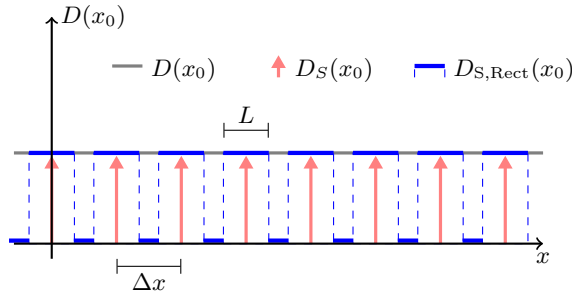


Fig. 6: Spatial discretization and reconstruction: continuous driving function $D(x_0)$, ideally sampled driving function $D_S(x_0)$ and reconstructed driving function $D_{\text{S,Rect}}(x_0)$ with the rect-function used as the postfilter.

L that stems from our chosen definition of a unit source Green's-like function which is independent of the piston's length. Inserting (21) and (36) into $D_{\text{S,Rect}}(k_x) = D_S(k_x, 0, z) \cdot H_{\text{Rect}}(k_x)$ of (24) we obtain

$$D_{\text{S,Rect}}(k_x) = \left[\frac{1}{\Delta x} \sum_{\mu=-\infty}^{+\infty} 2\pi \delta\left(k_x - \mu \frac{2\pi}{\Delta x}\right) \right] \times L \frac{\sin\left(\frac{k_x L}{2}\right)}{\frac{k_x L}{2}}. \quad (37)$$

Hence for $L = \Delta x$ follows

$$D_{\text{S,Rect}}(k_x) = \left[\sum_{\mu=-\infty}^{+\infty} 2\pi \delta\left(k_x - \mu \frac{2\pi}{\Delta x}\right) \right] \cdot \frac{\sin\left(\frac{k_x \Delta x}{2}\right)}{\frac{k_x \Delta x}{2}}. \quad (38)$$

The individual impulses in the Dirac comb with spacing $\Delta k_x = 2\pi/\Delta x = 2\pi/L$ are weighted by the sinc-function, for which finally

$$D_{\text{S,Rect}}(k_x) = \begin{cases} D(k_x) = 2\pi \delta(k_x) & \text{if } \mu = 0 \\ 0 & \text{otherwise.} \end{cases} \quad (39)$$

This proves the perfect reconstruction.

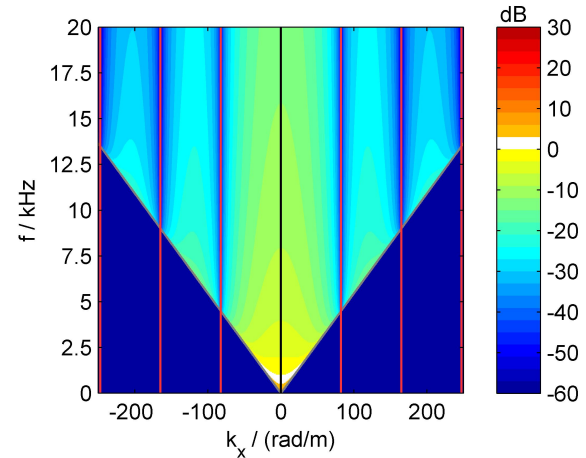


Fig. 7: $|G'_{\text{Rect}}(k_x)|$ for a line piston with length $L = 3'' = 0.0762$ m. $D_S(k_x)$ for an SSD discretization $\Delta x = L$ is indicated.

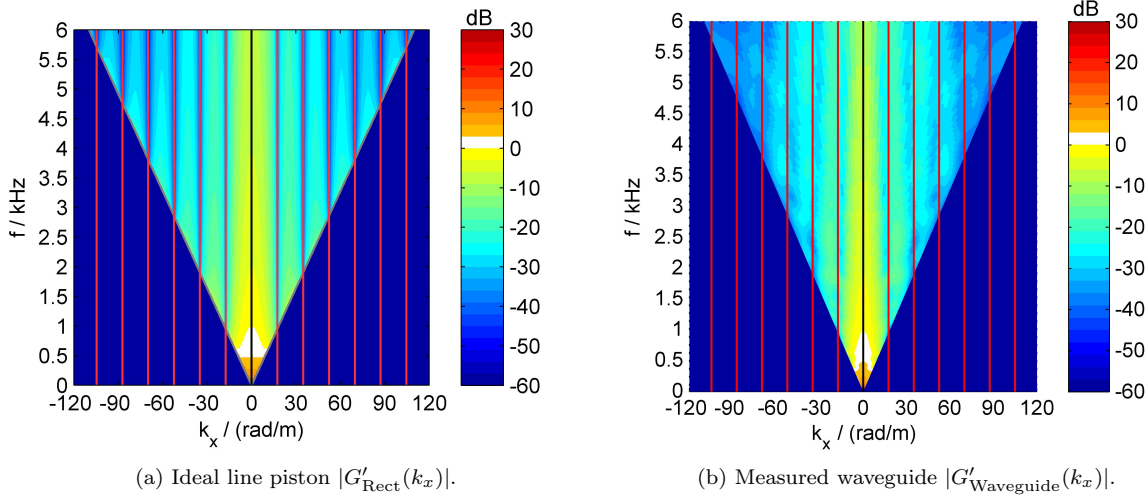


Fig. 8: $|G'(k_x)|$ and $D_S(k_x)$ with $\Delta x = L = 0.36$ m.

In fig. 7 the Green's-like function $G'_{\text{Rect}}(k_x)$ and $D_S(k_x)$ (21) are depicted for a line piston with length $L = \Delta x = 0.0762$ m. The intended driving function $D(k_x) = 2\pi\delta(k_x)$ is perfectly reconstructed and no spatial aliasing occurs. This is due to the complete suppression of the driving function's energy for $\mu \neq 0$ by the zeros of the sinc-term in the Green's-like function (38). Note that the zeros of the sinc-function are equidistantly spaced with $\Delta k_x = 2\pi/\Delta x$ which does not hold for the Bessel function $J_1(\cdot)$ that was used for circular pistons.

We conclude that the usage of a line piston is superior compared to a circular piston for high frequencies: In the ideal case all spatial aliasing energy is suppressed and the practical design is feasible.

Note that for $\Delta x > L$ (this case is depicted in fig. 6, cf. [3, fig. 6]) the repetitions exhibit smaller steps Δk_x compared to fig. 7. The spectral repetitions no longer coincide with the zeros of the Green's-like function. A criterion for tolerable aliasing contribution was introduced with the Active Radiation Factor (ARF) in [3, sec. 3.2]. For a large number of LSA elements the WST criterion 1 defines an $\text{ARF} = L/\Delta x \geq 0.82$ in order that aliasing contributions are at least 13.5 dB lower than that of the desired wave front. This is confirmed in our treatment. We can furthermore deduce that for a smaller chosen waveguide length L a potentially

smaller Δx – and therefore increased Δk_x – can be realized for an intended ARF. This might be useful for 'ARF<1'- LSA designs since the spatial aliasing energy is triggered at increased temporal frequencies leaving a larger frequency band uncorrupted from spatial aliasing. We do not propose a design criterion for the optimal waveguide length in this contribution and leave it for discussion in [21] due to the interaction of spatial discretization and truncation.

5.3. Reproduction with a Real Waveguide

This subsection examines the spatial lowpass characteristics of a commercial LSA element. An equiangular 2°-spherical balloon dataset of impulse responses from the single loudspeaker box was measured in the far- and freefield, cf. (27). The vertical isobars, i.e. the plane wave propagation angles $-\pi/2 \leq \theta \leq +\pi/2$ for $\varphi = \pi/2$ were extracted, smoothed in magnitude by 1/6 oct. and mapped to $k_x = \frac{\omega}{c} \sin \theta$. All frequency responses were normalized by the temporal spectrum of $k_x = 0$, therefore linearizing the spectrum on the main axis $\theta = 0$. This yields the reconstruction filter $H_{\text{Post}}(k_x) = H_{\text{Waveguide}}(k_x)$. Subsequently a 3 dB/oct. lowpass was applied to all spectra to obtain the Green's-like function $G'_{\text{Waveguide}}(k_x)$, cf. (31). This allows for direct comparison of the theoretical line piston Green's-like function (31),(33) with the measured one. For the interesting frequencies >1 kHz the

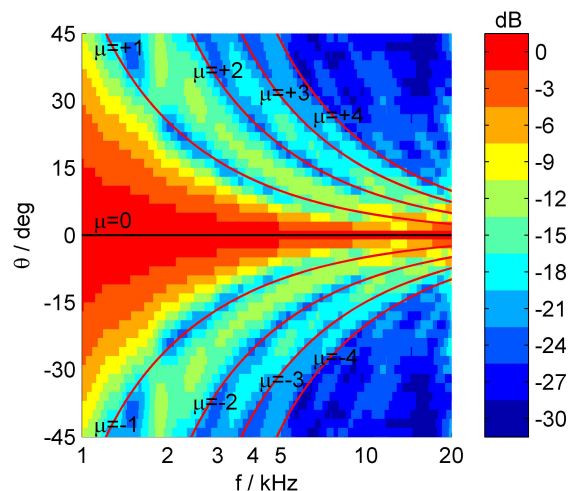


Fig. 9: Measured waveguide $|G'_{\text{Waveguide}}(k_x)|$ from fig. 8b as an isobar plot. Magnitude is normalized to $\theta = 0$. Hence the absolute attenuation values of the spatial aliasing energy contributions are presented. The spectral repetitions $|\mu| \leq 4$, $\mu \neq 0$ due to the discretized SSD are shown as red curves.

behavior of the measured waveguide can be considered as baffled due to the loudspeaker box dimension/wavelength ratio. Because of the nonlinear mapping $k_x = \frac{\omega}{c} \sin \theta$ the balloon dataset is not considered optimal for this examination. We rather suggest a measurement along a line and a subsequent spatial Fourier transform (5) to obtain an equidistant k_x -resolution, instead of an equiangular resolution, cf. [30, 31].

We assume a sampling distance $\Delta x = 0.36$ m due to the LSA element height, and an ARF=1. In fig. 8a the Green's-like function $G'_{\text{Rect}}(k_x)$ of an ideal waveguide corresponding to sec. 5.2 is depicted for $\Delta x = L$. In fig. 8b the measured Green's-like function $G'_{\text{Waveguide}}(k_x)$ is shown for comparison. The model and measurement are in good agreement.

An additional analysis with a common vertical isobar plot is conducted, which requires a remapping of the data in fig. 8b. The isobar plot is depicted in fig. 9 up to 20 kHz. We normalized all spectra to get a linearized, flat spectrum on its main axis (i.e. for $k_x = 0$, $\theta = 0$). The spatial-aliasing energy contributions are then given as absolute attenuation values within the surface plot. The black

horizontal line again represents the intended driving function. The repetitions $|\mu| \leq 4$, $\mu \neq 0$ are indicated with red curves. We recognize that the driving function repetitions are coincident with the zeros of the Green's-like function and thus will be suppressed. This confirms our modeling in sec. 5.2 and good spatial lowpass characteristics of the measured waveguide. Above 11 kHz the attenuation slightly becomes less than 10 dB for the first repetition $|\mu| = 1$. For $|\mu| > 4$ the Green's-like function attenuates the driving function repetitions > 20 dB. It is worth to note that fig. 9 does not visualize the directivity of a whole LSA but rather that of a single waveguide in its farfield.

6. CONCLUSION

The Wavefront Sculpture Technology criteria 1&2 for line source array design were reinforced by discussing the problem from a different viewpoint. Based on sound field synthesis fundamentals the sound field radiation from a discretized infinite linear source was described. The radiation synthesis problem was formulated for a continuous secondary source distribution. Spatially sampling of a suitable driving function models discrete loudspeaker positions. This sampling process was then discussed in the angular spectrum domain and the importance of a suitable postfilter was emphasized. In practice the used loudspeakers act as spatial reconstruction filters. By introducing loudspeaker directivities the WST criteria for required spatial-aliasing-free sound field reproduction with a line source array were confirmed. It was verified that for high frequencies a waveguide fulfills the criteria. An ideally operating waveguide modeled as a line piston with an active radiation factor of 1 completely suppresses all spatial aliasing energy. This ideal spatial lowpass characteristics has to be approached in practical waveguide designs. A real waveguide measurement was presented that complies with the criteria and is in good agreement with the proposed modeling. An alternative interpretation of commonly used vertical isobar plots of loudspeaker directivities was introduced.

7. ACKNOWLEDGEMENT

The authors would like to thank Anselm Goertz for providing the loudspeaker balloon dataset of the examined line source array loudspeaker box.

8. REFERENCES

- [1] Heil, C.; Urban, M. (1992): "Sound fields radiated by multiple sound sources arrays." In: *Proc. of 92nd Audio Eng. Soc. Convention, Vienna*, #3269.
- [2] Urban, M.; Heil, C.; Baumann, P. (2001): "Wavefront Sculpture Technology." In: *Proc. of 111th Audio Eng. Soc. Convention, New York*, #5488.
- [3] Urban, M.; Heil, C.; Baumann, P. (2003): "Wavefront Sculpture Technology." In: *J. Audio Eng. Soc.*, **51**(10):912–932.
- [4] Ureda, M.S. (2004): "Analysis of loudspeaker line arrays." In: *J. Audio Eng. Soc.*, **52**(5):467–495.
- [5] Jacob, K.D.; Birkle, T.K. (1990): "Prediction of the full-space directivity characteristics of loudspeaker arrays." In: *J. Audio Eng. Soc.*, **38**(4):250–259.
- [6] Gunness, D.W.; Hoy, W.R. (1999): "Improved loudspeaker array modeling." In: *Proc. of 107th Audio Eng. Soc. Convention, New York*, #5020.
- [7] Ahnert, W.; Baird, J.; Feistel, S.; Meyer, P. (2000): "Accurate electroacoustic prediction utilizing the complex frequency response of far-field polar measurements." In: *Proc. of 108th Audio Eng. Soc. Convention, Paris*, #5129.
- [8] Baird, J.; Meyer, P.; Meyer, J. (2001): "Far-field loudspeaker interaction: Accuracy in theory and practice." In: *Proc. of 110th Audio Eng. Soc. Convention, Amsterdam*, #5309.
- [9] Feistel, S.; Thompson, A.; Ahnert, W. (2009): "Methods and limitations of line source simulation." In: *J. Audio Eng. Soc.*, **57**(6):379–402.
- [10] Thompson, A. (2009): "Improved methods for controlling touring loudspeaker arrays." In: *Proc. of 127th Audio Eng. Soc. Convention, New York*, #7828.
- [11] Feistel, S.; Sempf, M.; Köhler, K.; Schmalle, H. (2013): "Adapting loudspeaker array radiation to the venue using numerical optimization of FIR filters." In: *Proc. of 135th Audio Eng. Soc. Convention, New York*, #8937.
- [12] Spors, S.; Rabenstein, R.; Ahrens, J. (2008): "The theory of Wave Field Synthesis revisited." In: *Proc. of the 124th Audio Eng. Soc. Convention, Amsterdam*, #7358.
- [13] Ahrens, J.; Spors, S. (2010): "Sound field reproduction using planar and linear arrays of loudspeakers." In: *IEEE Trans. Audio Speech Language Process.*, **18**(8):2038–2050.
- [14] de Vries, D. (1996): "Sound reinforcement by Wavefield Synthesis: Adaptation of the synthesis operator to the loudspeaker directivity characteristics." In: *J. Audio Eng. Soc.*, **44**(12):1120–1131.
- [15] Verheijen, E. (1997): *Sound Reproduction by Wave Field Synthesis*. Ph.D. thesis, Delft University of Technology.
- [16] Ahrens, J.; Spors, S. (2010): "An analytical approach to 2.5D sound field reproduction employing linear distributions of non-omnidirectional loudspeakers." In: *Proc. of 35th Intl. Conference on Acoustics, Speech and Signal Processing (IEEE 35th ICASSP), Dallas*, 105–108.
- [17] Koyama, S.; Furuya, K.; Hiwasaki, Y.; Haneda, Y. (2012): "Sound field reproduction method in spatio-temporal frequency domain considering directivity of loudspeakers." In: *Proc. of the 132nd Audio Eng. Soc. Convention, Budapest*, #8664.
- [18] Firtha, G.; Fiala, P. (2012): "Prefiltering the wave field synthesis operators - anti-aliasing and source directivity." In: *Intl. Conference on Noise and Vibration Engineering (ISMA 2012), Leuven, Belgium*, 3121 – 3136.
- [19] Hahn, N. (2013): "Sound field simulation using extrapolated impulse responses." In: *Proc. of the 52nd Audio Eng. Soc. Intl. Conference on Sound Field Control, Guildford*.
- [20] Lipshitz, S.P.; Vanderkooy, J. (1986): "The acoustic radiation of line sources of finite length." In: *Proc. of 81st Audio Eng. Soc. Convention, Los Angeles*, #2417.

-
- [21] Schultz, F.; Rettberg, T.; Spors, S. (2014): “On spatial-aliasing-free sound field reproduction using finite line source arrays.” In: *To be submitted*.
- [22] Skudrzyk, E. (1971): *The Foundations of Acoustics*. New York, Wien: Springer.
- [23] Kinsler, L.E.; Frey, A.R.; Coppens, A.B.; Sanders, J.V. (2000): *Fundamentals of Acoustics*. Hoboken: Wiley, 4. ed.
- [24] Meyer, P.; Schwenke, R. (2003): “Comparison of the directional point source model and BEM model for arrayed loudspeakers.” In: *Proc. of the Institute of Acoustics*, 25(4).
- [25] Williams, E.G. (1999): *Fourier Acoustics, Sound Radiation and Nearfield Acoustic Holography*. London, San Diego: Academic Press, 1. ed.
- [26] Olver, F.W.J.; Lozier, D.W.; Boisvert, R.F.; Clark, C.W. (2010): *NIST Handbook of Mathematical Functions*. Cambridge University Press, 1. ed.
- [27] Girod, B.; Rabenstein, R.; Stenger, A. (2001): *Signals and Systems*. Chichester: Wiley, 1. ed.
- [28] Mitchell, D.P.; Netravali, A.N. (1988): “Reconstruction filters in computer graphics.” In: *Computer Graphics*, **22**(4):221–228.
- [29] Ahrens, J.; Spors, S. (2010): “On the anti-aliasing loudspeaker for sound field synthesis employing linear and circular distributions of secondary sources.” In: *Proc. of the 129th Audio Eng. Soc. Convention, San Francisco*, #8246.
- [30] Pueo, B.; López, J.J.; Escolano, J.; Bleda, S. (2007): “Analysis of multiactuator panels in the space-time wavenumber domain.” In: *J. Audio Eng. Soc.*, **55**(12):1092–1106.
- [31] Koyama, S.; Furuya, K.; Hiwasaki, Y.; Haneda, Y. (2011): “Sound field recording and reproduction using transform filter designed in spatio-temporal frequency domain.” In: *Proc. of the 131st Audio Eng. Soc. Convention, New York*, #8544.